

GAS CONTENT AND KINEMATICS IN CLUMPY, TURBULENT STAR-FORMING DISKS

HEIDI A. WHITE^{1,2}, DAVID B. FISHER³, NORMAN MURRAY⁴, KARL GLAZEBROOK³, ROBERTO G. ABRAHAM^{1,2}, ALBERTO D. BOLATTO⁵, ANDREW W. GREEN⁶, ERIN MENTUCH COOPER⁷, DANAIL OBRESCHKOW⁸

Draft version July 6, 2021

ABSTRACT

We present molecular gas mass estimates for a sample of 13 local galaxies whose kinematic and star forming properties closely resemble those observed in $z \approx 1.5$ main-sequence galaxies. Plateau de Bure observations of the CO[1-0] emission line and *Herschel Space Observatory* observations of the dust emission both suggest molecular gas mass fractions of $\sim 20\%$. Moreover, dust emission modeling finds $T_{dust} < 30\text{K}$, suggesting a cold dust distribution compared to their high infrared luminosity. The gas mass estimates argue that $z \sim 0.1$ DYNAMO galaxies not only share similar kinematic properties with high- z disks, but they are also similarly rich in molecular material. Pairing the gas mass fractions with existing kinematics reveals a linear relationship between f_{gas} and σ/v_c , consistent with predictions from stability theory of a self-gravitating disk. It thus follows that high gas velocity dispersions are a natural consequence of large gas fractions. We also find that systems with lowest t_{dep} (~ 0.5 Gyr) have the highest ratios of σ/v_c and more pronounced clumps, even at the same high molecular gas fraction.

1. INTRODUCTION

Observations show that the majority of star formation in the universe occurs between $1 < z < 3$ (Hopkins & Beacom 2006; Madau & Dickinson 2014). When observed in the near infrared (NIR), star forming galaxies (SFGs) at this epoch are frequently irregular or “clumpy” in morphology and H α fluxes suggest elevated star formation rates (SFRs; typically $\sim 10^2 M_\odot \text{ yr}^{-1}$) reminiscent of local merging systems. Integral-field spectroscopy (IFS) surveys of rest-frame optical emission lines report that despite the morphology, the kinematics of these galaxies better resemble rotating, but turbulent, disks: a large fraction of these systems exhibit ordered rotation and are observed to sit on the star-forming main sequence. Spatially-resolved observations reveal that the bulk of these systems have high internal velocity dispersions ($\sigma \approx 20 - 100 \text{ km/s}$) when compared to $z \sim 0$ galaxies (see Förster Schreiber et al. 2009; Genzel et al. 2008; Wisnioski et al. 2011, 2015). Moreover, these systems are distinct from local star forming spirals in that they are consistently observed to contain substantial molecular gas fractions ($f_{gas} \sim 20\text{-}50\%$; Tacconi et al. 2010,

2013; Daddi et al. 2010).

A significant fraction of star formation within high-redshift clumpy galaxies occurs in large, massive clumps (kpc-scale, $\sim 10^9 M_\odot$). Fisher et al. (2017a) shows that the detailed properties of clumps in turbulent disks are best described by predictions from self-gravitating instabilities within disk galaxies (as opposed to mergers or other instabilities). This theory (see Dekel et al. 2009) suggests that the amplitude of instabilities is governed by three forces: (1) gravitational forces scaling with the surface density of the gas, (2) turbulent pressure forces due to the velocity dispersion and (3) shear forces caused by the differential rotation of the disk. The balance between these forces is suitably measured by the non-dimensional parameter Q (Toomre 1964), such that $Q > 1$ regions are stable, whereas $Q < 1$ regions are unstable and form clumps. According to this model, the high gas fractions observed in high- z disks (e.g. Elmegreen et al. 2009) are, at least partially, responsible for the apparent widespread instabilities of these high- z disks. In turn, the high velocity dispersions (a stabilizing force) are commonly used to explain the large size of the clumps following Jeans theory. Moreover, if this mechanism is indeed the primary force in producing clump formation, it’s certain to play an important role in the feedback cycle within galaxies: e.g. the release of gravitational potential energy as massive clumps form, torques felt between in-spiraling clumps, and energy injection from star formation are all likely to contribute to high velocity dispersions of the ISM (Bournaud & Elmegreen 2009; Lehnert et al. 2009; Genzel et al. 2008, 2011).

Although the groundwork for this theory has existed for some time (Dekel et al. 2009), it has just begun to be tested observationally. Truly robust tests of this instability argument requires observations of the internal properties of a sample of galaxies - gas mass fractions and resolved kinematics. Direct observation presents substantial challenges as these clumpy star forming systems are almost entirely unique to the high- z universe and are, thus, quite difficult to observe. Resolving the kine-

¹ Department of Astronomy and Astrophysics, University of Toronto, 50 St. George St., Toronto, ON, M5S 3H8, Canada

² Dunlap Institute for Astronomy and Astrophysics, University of Toronto, 50 St. George St., Toronto, ON, M5S 3H8, Canada

³ Centre for Astrophysics and Supercomputing, Swinburne University of Technology, P.O. Box 218, Hawthorn, VIC 3122, Australia

⁴ Canadian Institute for Theoretical Astrophysics, 60 St. George Street, University of Toronto, Toronto ON M5S 3H8, Canada

⁵ Department of Astronomy and Joint Space Institute, University of Maryland, College Park, MD 20642, USA

⁶ Australian Astronomical Observatory, P.O. Box 970, North Ryde, NSW 1670, Australia

⁷ Astronomy Department, University of Texas at Austin, Austin, TX 78712, USA

⁸ International Centre for Radio Astronomy Research (ICRAR), University of Western Australia, M468, Crawley, WA 6009, Australia

matics of the star forming and molecular regions within $1 < z < 3$ disks is challenging due to observational limitations: e.g. seeing/atmospheric effects, low signal-to-noise ratio (SNR). Both NIR and molecular gas observations at high- z require long integration times to ensure detection and, at present, while there exist ~ 200 galaxies with gas fractions at high- z , only a handful have measured resolved kinematics (primarily those with overlap in the PHIBSS & SINS samples). These high- z galaxies are also chosen to be very bright, necessarily biasing high- z observations.

An increasing number of studies focus on overcoming issues of distance by identifying rare, nearby galaxies with properties similar to high redshift main-sequence galaxies. Other groups have also identified large gas fraction systems using atomic gas (Garland et al. 2015; Catinella & Cortese 2015). Green et al. (2014) presented DYNAMO, a sample of 95 local ($z \sim 0.06 - 0.08$ & $0.12 - 0.16$) galaxies whose kinematic and star formation properties closely resemble that observed in high- z clumpy disks (see Green et al. 2014, Bassett et al. 2014, Fisher et al. 2017b). Green et al. use an inverted Kennicutt-Schmidt relation to estimate the total gas content ($f_{gas,tot}$) for galaxies in DYNAMO and find evidence of a correlation with σ/v_c . Confirmed detections of CO[1-0] emission in four DYNAMO targets by Fisher et al. (2014) argues that at least some fraction of the sample are also gas rich ($f_{gas} \sim 20-30\%$).

In this paper, we analyze the ISM properties of clumpy, turbulent disk galaxies. We present molecular gas fractions for 13 DYNAMO galaxies. We utilize two, separate methods for inferring f_{gas} to limit methodological bias and maximize the sample size. We then couple this new information with existing high-resolution integral field spectroscopy (IFS) to investigate the Toomre instability argument and quantify the relationship between the molecular gas content and ionized gas kinematics.

The paper is structured as follows: in §2, we provide a comparison of our DYNAMO sample with systems observed at high- z . In §3, we discuss our IR and CO[1-0] observations and describe the two methods utilized in estimating molecular gas and dust masses for our sample. Finally, in §4, we present our results and discuss them in context, and in §5, summarize our major findings.

2. SAMPLE

The targets in this paper are a subset of the greater DYNAMO sample (originally presented in Green et al. 2014, hereafter referred to as DYNAMO-I). DYNAMO is an H α IFU survey of local ($z \sim 0.1$) galaxies which have been selected (in two SDSS redshift windows) to be H α -luminous (top 1% in the local universe, based on fiber luminosity; $SFR \sim 11 M_{\odot} \text{ yr}^{-1}$). The majority of stellar masses of our sample fall between $1-5 \times 10^{10} M_{\odot}$ (see Fig.1).

2.1. DYNAMO systems resemble $z=1.5$ main-sequence galaxies

A large fraction ($\sim 84\%$) of DYNAMO galaxies appear disk-like and about half are located on the Tully-Fisher relation (Green et al. 2014). Spatially resolved spectroscopy of redshifted H α emission in DYNAMO-I reveals enhanced velocity dispersions ($20-100 \text{ km s}^{-1}$;

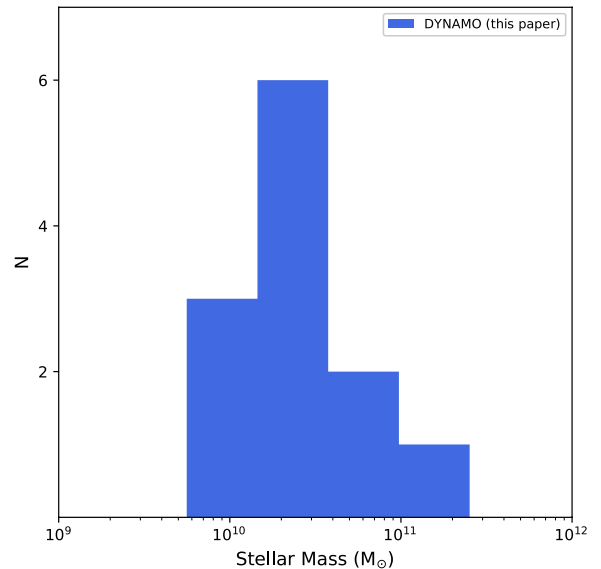


Figure 1. The distribution of stellar masses for the DYNAMO galaxies presented in this paper. The majority of the targets within our sample range between masses of $1 - 5 \times 10^{10} M_{\odot}$.

Green et al. 2014, Bassett et al. 2014, Bekiaris et al. 2016) and evidence of ordered, rotating disk structure. Bassett et al. (2014) follow up on these findings by Green et al. (2010, 2014) with higher resolution and more sensitive kinematics from Gemini/GMOS to confirm DYNAMO galaxies are rotating in both gas and stars.

DYNAMO targets also appear gas rich. Fisher et al. (2014) performed CO[1-0] observations using the Plateau de Bure interferometer (PdBI) for four DYNAMO targets (with three successful detections) and report gas mass fractions between 20-30%. Comparison with typical local spirals of similar stellar mass ($f_{gas} \sim 1-8\%$; Saintonge et al. 2011a) suggests that the DYNAMO galaxies comprise a very gas rich subset of the local star forming population.

Similar to systems at high- z (e.g. Genzel et al. 2011; Wisnioski et al. 2015) star forming disks in DYNAMO appear not only turbulent, but clumpy. High-resolution ($\sim 100 \text{ pc}$) Hubble Space Telescope (HST) follow up of the clumps by Fisher et al. (2017b) confirm that they are both large ($\overline{d_{core}} \sim 0.5 \text{ kpc}$) and massive ($\sim 10^{8-9} M_{\odot}$). Moreover, adaptive optics (AO)-corrected IFS observations verify that the observed high σ values are consistent down to sub-clump ($\sim 100-200 \text{ pc}$) scales (Oliva-Altamirano et al., *submitted*).

Fisher et al. (2017b) find that DYNAMO disks are compact and their H α half-light radii are most similar to those observed at $1.5 \leq z \leq 2$. While in local systems, typical SFR surface densities (Σ_{SFR}) range from 10^{-4} - $10^{-1} M_{\odot} \text{ yr}^{-1} \text{ kpc}^{-2}$, Fisher et al. (2017b) also show that Σ_{SFR} in DYNAMO is orders of magnitude greater ($\sim 1-10 M_{\odot} \text{ yr}^{-1} \text{ kpc}^{-2}$) and best matched to that found in systems at $1 < z < 3$.

A plausible interpretation of DYNAMO galaxies is that their striking similarity with $z \sim 1.5$ main-sequence disks

is because a similar internal physical mechanism is driving the star formation and kinematics in both objects. Indeed, Green et al. (2014) and Fisher et al. (2017b) find that DYNAMO galaxies lie close to the $z \sim 1.5 - 2.0$ star formation rate-stellar mass main sequence. The key difference between these two populations, however, is not the internal physics, but rather the frequency of that mechanism at $z > 1$ and at $z = 0.1$. DYNAMO galaxies are then excellent laboratories for studying a major mode of high- z star formation (at a critical epoch) on higher signal-to-noise data.

2.2. Classifying DYNAMO galaxies as mergers or disks

Constraining the fraction of mergers within our sample has important implications for our choice of α_{CO} and our interpretation of these DYNAMO galaxies as clumpy, turbulent disks. All of the targets in this paper have been observed to have kinematic signatures that best resemble disks (i.e. rotation and a somewhat uniform velocity dispersion field; see Green et al. 2014 and Bekiaris et al. 2016). As we mention above, Green et al. (2014) show that the kinematics in DYNAMO galaxies are consistent with the Tully-Fisher relationship.

Fisher et al. (2017b) use HST 600nm continuum maps to show that the surface brightness profiles of 8 of 10 DYNAMO galaxies in their sample are well described by an exponential decay with increasing radius, which is consistent with disks. Seven of these galaxies make up over half of the sample discussed in this paper (G14-1, D15-3, D13-5, C13-1, G20-2, G08-5, G04-1).

Classification of disks and mergers in galaxies with as high gas fractions and star formation rates as DYNAMO is of course an imperfect process. Moreover, the classification of ‘‘turbulent disks’’ is relatively new. Nonetheless, we expect (based on our previous results) our classifications to be accurate at the $\sim 80\%$ level.

3. GAS CONTENT AND KINEMATICS

3.1. M_{gas} Determinations

There are significant challenges to directly observing molecular gas within galaxies. The H_2 molecule, while abundant, has no dipole moment and its lowest vibrational state is difficult to excite at typical molecular cloud temperatures (10-20K; Kennicutt & Evans 2012). Consequently, inferring a galaxy’s molecular gas content is most often performed via indirect measurements. In this paper, we use two common methods:

- Observations of ground state CO[1-0] rotational line emission allow for determination of a CO line luminosity for the galaxy. Then, using locally-derived empirical values for α_{CO} , this CO luminosity is converted to an estimate for the system’s molecular gas mass (M_{mol}) and, subsequently, the inferred baryonic gas fraction ($f_{\text{gas}} = M_{\text{mol}} / (M_{\text{mol}} + M_{\text{star}})$).
- Available IR-band flux information from Herschel PACS+SPIRE is fit with a modified blackbody model to constrain the dust mass (M_{dust}), which is then used to infer a gas mass via the metallicity-dependent empirical dust-to-gas ratio.

3.1.1. CO(1-0) Observations

Six galaxies (C13-1, G20-2, G13-1, G14-1, G08-5, and D15-3 from DYNAMO-I) were observed on May 20, 23, & 27-29 of 2014 (PID 12977, PI Damjanov) for a combined period of 7.5 hr using the PdBI targeting emission within the 3-mm atmospheric window (80 - 116 GHz) via the CO(J=1→0) transition. Observations were carried out using 5 antennas (in ‘D’ configuration) and resulted in synthesized beams around $6'' \times 4.5''$ in size. Due to the declination of some of our sources and incomplete (u,v) coverage, some of our maps exhibit elongated beams and side-lobe structure (see Fig. 2). However, this does not significantly affect the measurement of total flux.

The data were calibrated on-site using the *CLIC* package of the IRAM GILDAS data reduction software and typical flagging (Guilloteau & Lucas 2000). Images were deconvolved using the *MAPPING* package on the calibrated visibility tables. The Clark cleaning algorithm was utilized to construct our clean map. Our data was processed with between 50-100 iterations, natural weighting for coverage points within our (u,v) grid, a default velocity bin width of 28 km s^{-1} , and an average cell size of $1.3''$ for our 128×128 image. For G20-2, G13-1, G14-1, & G08-5, the emission line signal-to-noise ratio (SNR) was low enough (< 5) to require re-binning in velocity space to 119 km s^{-1} . Typical RMS flux values within the resultant cubes were $2\text{-}3 \text{ mJy beam}^{-1}$ (exact flux errors in Table 1). The observations discussed above build upon a sample from a previous program (X02C in the June-November 2013 period; see Fisher et al. 2014).

Emission line analysis for our mm-wavelength observations was done using the Common Astronomy Software Applications (CASA)’s spectral line tool. For each target, we extracted spectra using a beam-size aperture (except for C13-1 and D15-3, which required larger apertures due to being marginally-resolved) and directly integrated over our CO[1-0] line to obtain an upper limit estimate for the velocity integrated flux (F_{CO} ; in Jy km s^{-1}). The CO emission lines for our two lowest-redshift targets (C13-1 & D15-3; $z \sim 0.07$) exhibit a ‘double-peaked’ line-shape (see Fig. 2, row 3). For these two targets we have included position-velocity diagrams in Fig. 2.

To estimate upper limits for the molecular gas masses and implied mass fractions ($f_{\text{gas}} = M_{\text{gas}} / (M_{\text{gas}} + M_*)$) we used the following expression (similar to Tacconi et al. 2013):

$$M_{\text{gas}} = 1.75 \times 10^9 \left(\frac{\alpha_{\text{CO}}}{4.36} \right) F_{\text{CO}} R_{\text{J1}} \lambda_{\text{obs}}^2 D_{\text{L}}^2 (1+z)^{-3} \quad (1)$$

where F_{CO} is the CO[1-0] flux in Jy km s^{-1} , R_{J1} is the transition coefficient (equal to 1 for the ground-state), λ_{obs} is the observed wavelength in mm, and D_{L} is the luminosity distance in Gpc. We note that this formula incorporates a correction for the 36% increase due to the Helium fraction of molecular clouds. Similar to Fisher et al. (2014), we assume the following H_2 mass-to-CO luminosity ratio (α_{CO} ; see Bolatto et al. 2013 for a thorough review of this ratio for all galaxy populations):

$$\alpha_{\text{CO}} = M_{\text{gas}} / L'_{\text{CO}} \approx 3.1 M_{\odot} (\text{K km s}^{-1} \text{ pc}^2)^{-1} \quad (2)$$

for our six targets. While we acknowledge that choice

of α_{CO} is decisive in determining whether or not the galaxies appear gas rich, we point out that our assumed value is slightly conservative and defend this high redshift choice for DYNAMO systems using arguments presented in §2. (As we will see in §4.1, our T_{dust} estimates directly support this choice of α_{CO} .) The gas consumption timescale was estimated as $t_{\text{gas}} = M_{\text{gas}}/\text{SFR}$. Observed fluxes and line widths can be found in Table 1; inferred values for M_{gas} and f_{gas} , can be found in Table 2.

3.1.2. *Herschel IR Observations*

Four DYNAMO galaxies (D00-2, D13-5, D15-3, and G03-2) were observed in July 2012, using *Herschel*'s PACS instrument in the 70 and 160 μm wavebands. The raw data was extracted from the *Herschel* Science Archive and reduced & analyzed using ESA's *Herschel* Interactive Processing Environment (HIPE; Ott 2010) software and the current version of the reduction pipeline. Fluxes values were estimated using HIPE's *annularAperturePhotometry* module coupled with the suggested aperture sizes stated in the HIPE data reduction manual⁹. Flux values were re-scaled via aperture corrections given in Balog et al. (2014) to account for lost light due to a fixed aperture size. The quoted errors in flux were estimated using ESA's HIPE software which averages background noise levels within a similar region size, but offset 10'' from the target.

Five additional DYNAMO galaxies (C08-2, I09-1, C14-2, D14-1, and G14-1) were observed as part of the *Herschel* ATLAS (hereafter, H-ATLAS; Eales et al. 2010) survey. H-ATLAS targets have observations with both PACS (100 & 160 μm) and SPIRE (250, 350, & 500 μm) cameras. For these galaxies fluxes have been extracted directly from the H-ATLAS catalog (Bourne et al. 2016). Details on data reduction and flux estimation for these targets can be found in Eales et al. (2010).

3.1.3. *Single-T "Greybody" Fitting*

Dust mass has been shown to be an excellent tracer of hydrogen gas mass (reviewed in Bolatto et al. 2013). Dust emission in galaxies is commonly modeled via a single temperature modified blackbody (also known as a "grey body") approximation. Modelling the dust in this manner makes two noteworthy assumptions: 1) that all dust grains share a common temperature and 2) the dust distribution is optically-thin. In recent years, spectral energy diagram (SED) fitting methods have been developed which fit more complex dust models - namely those in which the dust grains are represented by a range of temperatures (e.g. Draine & Li 2007).

In this paper, we fit the following equation, representing a modified blackbody, to the *Herschel* data:

$$f_{\nu} = \frac{M_{\text{dust}}}{D_L^2} \kappa_{\text{abs}} B_{\nu}(T_{\beta}) \quad (3)$$

where D_L is the luminosity distance, κ_{abs} is the emissivity (or the absorption coefficient, where $\kappa_{\text{abs}} = \kappa_0(\lambda_0/\lambda)^{\beta}$), B_{ν} is the Planck function for a single-temperature dust model, and T_{β} & M_{dust} are left as fitted parameters. Surveys of the far-infrared *Herschel* colors of galaxies have revealed that $1 \leq \beta \leq 2$ (Boselli

et al. 2012; Auld et al. 2013; Bianchi 2013). For this work, we adopt a $\beta=1.5$ value consistent with that in Draine & Li (2007). Example fits for I09-1 and D15-3 are given in Fig.3.

In the paragraphs that follow, we outline the uncertainties introduced by estimating the dust mass (and, similarly, the gas mass) in this manner.

The largest source of uncertainty in the greybody dust model is the assumption of a single temperature for all dust emission. Galaxies likely have a range of dust temperatures (Draine & Li 2007). Emission from $\sim 20 - 150\mu\text{m}$ is dominated by warm dust mostly heated by young stars. Emission at longer wavelengths may be driven by lower energy photons, and may have lower temperatures. This introduces a systematic uncertainty in the mass estimates we derive from this technique as it does not explicitly account for contributions from a cold dust (10 - 15K) component. Recent comparisons of the full-SED and modified blackbody methods (e.g. Cortese et al. 2012; Bianchi 2013; Berta et al. 2016) reveal that the modified blackbody model systematically underestimates M_{dust} by 20-50% compared to Draine & Li (2007) models. We therefore acknowledge that the dust (and, similarly, gas) mass estimates for our *Herschel* sample may be greater than those presented here.

As we discuss above, not all galaxies in our *Herschel* sample have the same wavelength coverage for the IR SED. To account for this greybody fits for H-ATLAS targets were re-processed with solely the 100 & 160 μm fluxes and this resulted in estimates for M_{dust} and T_{dust} that were in agreement (to the 5-point fitted values) within $\sim 20\%$.

Use of a Galactic dust-to-gas ratio has a number of limitations. Firstly, there is significant uncertainty in its value: observations of solar metallicity galaxies (such as DYNAMO) produce dust-to-gas ratios which exhibit a scatter of about 0.4 dex (Rémy-Ruyer et al. 2014). Moreover, the mass inferred from dust conversion represents a galaxy's *total* gas content, whereas CO emission specifically traces the molecular gas (see §3.1.1). To date, the H_2/HI ratio in gas rich disks remains poorly constrained and while typical values of H_2/HI in local spirals is about 1/3 (Saintonge et al. 2011b), in high- z disks it may be closer to parity (Obreschkow & Rawlings 2009). We also acknowledge that assumption of a universal dust-to-gas ratio across our sample is likely too simplistic and might bias our result. In light of such, we estimate that a more realistic uncertainty in our dust results is $\sim \pm 0.3$ dex (around a factor of 2).

Despite these caveats, Genzel et al. (2015) find that, on average, CO and dust techniques provide consistent gas mass estimates of galaxies across a range of redshifts (see their Eq. 2). DYNAMO galaxies G14-1, D15-3, and D13-5 fall within both our IR and CO samples (D13-5 CO values from Fisher et al. 2014) and estimates for their molecular gas masses using both techniques are in good agreement (within a few percent). Therefore, we adopt the same formula (e.g. Equation 2) as well as a similar conversion factor (D:G=0.01) to convert our fitted dust values to gas masses. Final M_{gas} estimates (with errors) and corresponding f_{gas} values can be found in Table 2.

3.2. *System kinematics and SFRs*

⁹ Wiki - <http://herschel.esac.esa.int/hcss-doc-14.0/index.jsp>

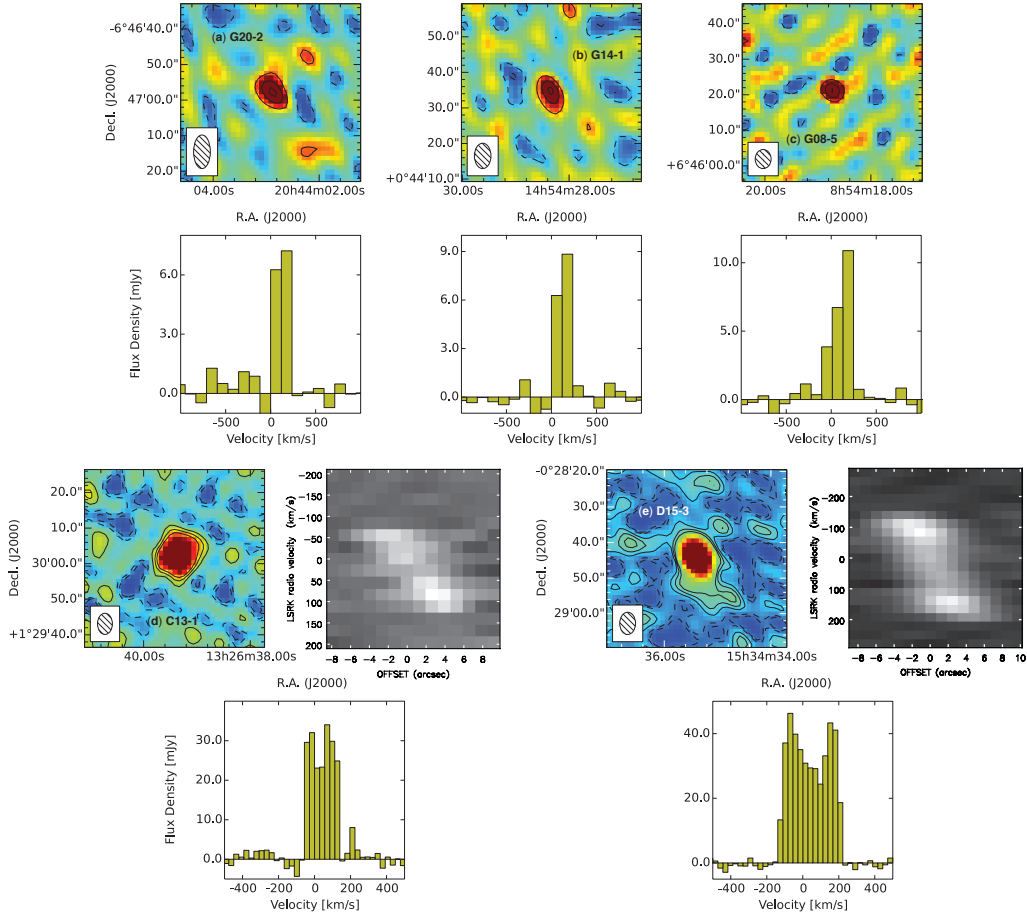


Figure 2. Emission maps (rows 1 & 3) and spectra (rows 2 & 4) for the five galaxies detected with PdBI. All emission maps are $50'' \times 50''$ and produced by collapsing across the CO[1-0] linewidth; 2-, 4-, & 6- σ contours and individual synthesized beams have been included for reference. Below each emission map, we include corresponding spectra of the detected CO[1-0] line referenced to the expected redshift velocity. Spectra have bin-sizes of 119 km s^{-1} for galaxies G20-2 (a), G14-1 (b), & G08-5 (c) and 28 km s^{-1} for galaxies C13-1 (d) & D15-3 (e). The two $z \sim 0.07$ systems (d & e) are marginally resolved by the beam and exhibit clear kinematic structure both on-sky and in the spectra. For these two galaxies, we have included position-velocity diagrams in row 3.

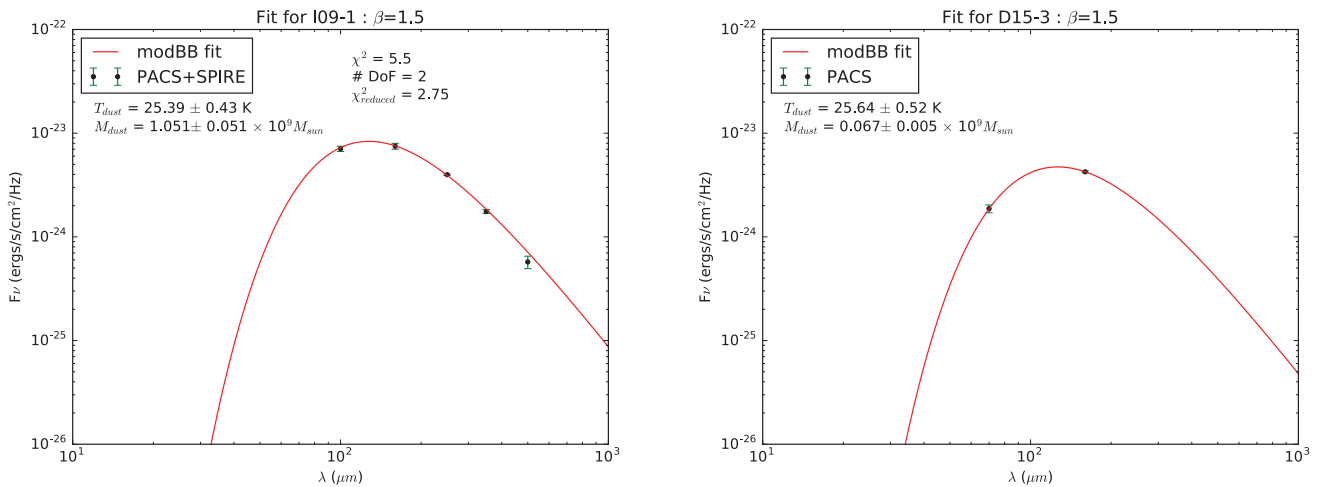


Figure 3. For 9 of the 13 galaxies presented in this paper, dust masses obtained from fitting a modified blackbody model to the *Herschel* waveband data were used to infer the gas mass. Here, we show example fits (I09-1 and D15-3) for which we have chosen $\beta=1.5$. For our sub-sample of DYNAMO galaxies observed with *Herschel*, we consistently find $T_{\text{dust}} < 30\text{K}$ and dust masses which suggest $f_{\text{gas}} \sim 10\text{-}40\%$.

For 9 of the 13 galaxies discussed in this paper, we utilize the kinematic modeling results of Bekiaris et al. 2016. The authors refer readers interested in a more

in-depth discussion on the methodology for determining kinematic properties of galaxies in DYNAMO to Bekiaris et al. 2016. The global gas velocity dispersion (σ) and rotational velocity (v_c) values included in our analysis (listed in Table 2) have been extracted directly from the Table C2 in Bekiaris et al. (2016) (note: v_c is taken to be $V_{2.2R}$). For one galaxy, G08-5, we use kinematic values obtained from disk modelling of high-resolution Gemini maps (Fisher et al. 2017b).

All of the DYNAMO galaxies in our sample have IR observations using the Wide-field Infrared Survey Explorer (mission paper by Wright et al. 2010; data available at <http://irsa.ipac.caltech.edu/Missions/wise.html>). To estimate star formation rates, we use Equation 2 from Lee et al. (2013) and flux values from WISE band-4. SFRs for our sample of galaxies are listed in Table 2.

4. RESULTS & DISCUSSION

Estimates for gas mass (M_{gas}) and gas mass fraction (f_{gas}) for the 12 detected targets in our sample (we provide an upper limit for G13-1) are found in Table 2. We report average f_{gas} values of 0.20 and 0.23 for the systems with PdBI CO[1-0] and *Herschel* data, respectively. Consistent with this, we find $\langle f_{gas,H-ATLAS} \rangle = 0.25$ and $\langle f_{gas,PACS} \rangle = 0.22$. This suggests excellent agreement between the two estimation techniques and is consistent with previous work on the sample ($\langle f_{gas} \rangle = 0.2$, from Fisher et al. 2014). In all cases, the gas mass estimates fall below the estimated dynamical mass values (derived using $v(r) = V_{2.2}$ and $r = 2.2 \times r_{1/2,r}$ from Bekiaris et al. 2016) and, in most cases, the implied gas mass comprises about 10-15% of the system mass.

Of the 12 detected galaxies, D15-3 has the lowest reported gas fraction ($\sim 11\%$) and G03-2 the highest ($\sim 44\%$). The mean value for molecular gas fraction in blue-sequence $z = 0$ galaxies is about 4%. Total gas is a factor of a few larger following COLDGASS, see Saintonge et al. 2011b. This shows that DYNAMO galaxies have substantially higher molecular gas content presumably fueling their higher rates of star formation.

We do not observe a significant emission source in the CO map for G13-1. We place upper limit constraints on its molecular gas mass. We measure an upper limit to CO(1-0) flux of $0.149 \text{ Jy km s}^{-1}$. Using the same α_{CO} as in Equation 1 implies an $f_{gas} < 4\%$. Thus, we find G13-1 to be comparatively gas-poor with respect to its fellow DYNAMO members, and more in line with what is routinely observed in local SFGs (Saintonge et al. 2011b). Moreover, the lower CO flux per unit SFR of G13-1 is consistent with the interpretation of this galaxy as a merger based on both kinematic and HST morphology (Fisher et al. 2017b). Similarly, DYNAMO galaxy H10-2 was undetected by Fisher et al. (2014) and subsequently determined with the same morphological and kinematic analysis to be more consistent with advanced stage merging galaxies.

In DYNAMO-I, Green et al. use the Kennicutt-Schmidt law, which defines the relationship between a galaxy's surface density of gas and star formation, to report estimates for the total (HI + H₂) gas content of the sample. The molecular gas fraction reported in this paper seem to suggest that the majority ($\sim 40\text{-}70\%$) of the gas content is molecular. We interpret this as a likely consequence of the fact that DYNAMO observations of

star forming regions probe within the inner part of the disk where (as seen in Leroy et al. 2008) the gas content is mainly H₂-dominated. Alternatively, the galaxies may be so gas enriched that the hydrogen gas over a larger fraction of the disk doesn't remain in the atomic phase, but instead transitions into the molecular state (due to increasing density); beyond $\Sigma_{gas} \sim 10 \text{ M}_{\odot}/\text{pc}^2$ pressure allows HI to transition into H₂. Within DYNAMO, average gas densities are observed to be well above this threshold.

As stated in §3, two of the lower redshift targets observed with PdBI were marginally-resolved. This allows for the construction of position-velocity diagrams (seen for C13-1 and D15-3 in Fig. 5). The rotational velocities determined by Green et al. (2014) are a factor of $\sim 1.5x$ higher than that suggested by the CO kinematics (even correcting for inclination); this is likely due to the fact that, again, the observed CO emission is probing only the inner part of the disk (Leroy et al. 2008).

4.1. Cold dust within DYNAMO galaxies?

The average T_{dust} for DYNAMO galaxies measured in this paper is $27.5 \pm 0.52 \text{ K}$. There is excellent agreement between the H-ATLAS and PACS-only samples: we find $\langle T_{dust} \rangle = 27.16 \pm 0.87 \text{ K}$ and $27.76 \pm 0.58 \text{ K}$, respectively. The highest value for T_{dust} in DYNAMO galaxies measured in this paper is $\sim 30 \text{ K}$.

We use the IR-band information to evaluate the total IR luminosity for DYNAMO systems (Galametz et al. 2013, Eq. 3 & Table 3) and in Fig. 4, we compare the dust temperature and luminosity of DYNAMO galaxies to other characteristic samples. Local spirals have similar dust temperatures as DYNAMO galaxies, with $\langle T_{dust} \rangle \sim 26.8 \pm 0.71 \text{ K}$ (Skibba et al. 2011). However, these local spirals are typically 1-2 orders of magnitude fainter in IR luminosity. In the local Universe, systems with similar IR luminosities (and hence similar SFR) to that of DYNAMO galaxies have average dust temperatures that are $43.2 \pm 2.1 \text{ K}$ (Yang et al. 2007). This is because those starbursts are mostly very concentrated, because they come from mergers, for example. This is considerably (about a factor of two) higher than that observed in DYNAMO galaxies. These results argue for the presence of cold dust within DYNAMO systems and suggest that a greater fraction of the interstellar dust is not being heated as it is in $z = 0$ galaxies with similar star formation rates.

Yang et al. (2007) suggest that the high dust temperatures observed in their sample is a consequence of the compact nature of the IR emission. Here we derive a simple and straightforward relationship between the dust temperature and fundamental galaxy parameters.

We begin with the Stefan-Boltzmann Law:

$$F = \sigma_b T_{\text{eff}}^4 = \frac{L}{2\pi R_d^2} \quad (4)$$

which can be solved for the effective temperature (T_{eff}). This is then re-arranged to the following form:

$$T_{dust} \approx T_{\text{eff}} = \left(\frac{L}{2\pi R_d^2 \sigma_b} \right)^{1/4} \quad (5)$$

where σ_b is the Stefan-Boltzmann constant (in cgs units),

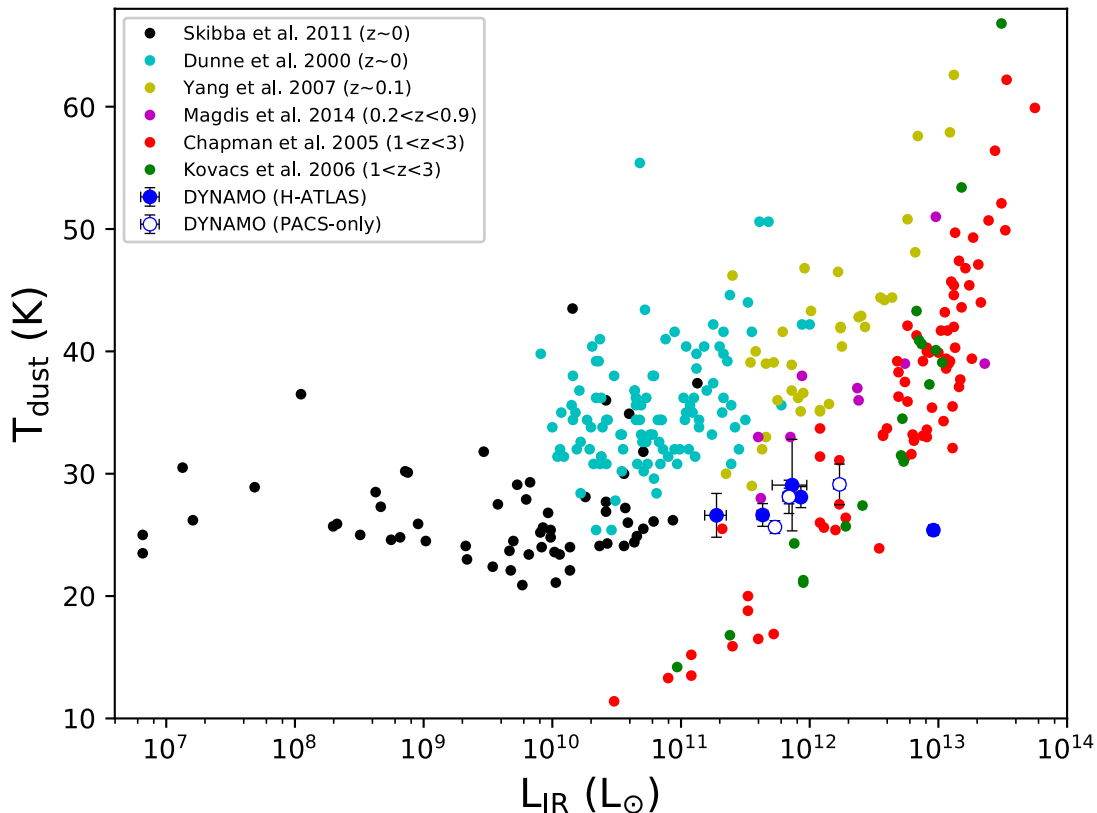


Figure 4. DYNAMO galaxies (blue open and closed circles, with errors) are IR luminous, yet exhibit cold dust temperatures. We derived T_{dust} values using the modified blackbody equation in §3.1.3 (Eq. 3) and total IR luminosities were estimated from Herschel PACS+SPIRE fluxes (Galametz et al. 2013; Eq. 3). Adapted from Fig. 3 in Hwang et al. (2010), we include galaxies from KINGFISH (black circles; Skibba et al. 2011), IR-luminous galaxies at $z \sim 0$ (cyan; from Dunne et al. 2000), intermediate redshifts (Yang et al. 2007 in yellow, Magdis et al. 2014 in magenta) and sub-mm galaxies (SMGs; red, from Chapman et al. 2003 & Kovács et al. 2006, in green) for reference.

R_d is a characteristic radius for the disk, and L is the dust luminosity (defined as $L = \text{SFR} \times \epsilon c^2$, where $\epsilon = 8 \times 10^{-3}$ for a Kroupa or Chabrier initial mass function). One then finds that a galaxy’s dust temperature should roughly scale with its star formation rate and disk size:

$$T_{dust} \propto \text{SFR}^{1/4} R_d^{-1/2}. \quad (6)$$

The above proportionality implies that the bulk of the dust in galaxies with colder dust temperatures is on average more distant from the radiation source. More generally, the dust temperature is a function of the local interstellar radiation field. If the star formation is distributed throughout these galaxies and the SFR density is lower then the temperatures will be colder. The dust in DYNAMO galaxies is then likely more extended than one might expect in a typical ULIRG at $z = 0.1$ with the same SFR. DYNAMO systems are selected to be rotating (ie. disks), a criterion not imposed on the sample presented in Yang et al. (2007). Therefore, dust in DYNAMO systems are likely (on average) less compact and, consequently, less heated.

In local spirals (for example, KINGFISH survey galaxies) the Jeans length is comparatively small - thus, collapse occurs more readily and the dust is mostly located

in regions where stars are actively forming. This is not assumed to be the case for the DYNAMO galaxies presented here, whose higher gas velocity dispersions predict larger Jeans lengths.

We conclude by noting that the state of the ISM of turbulent disks in the DYNAMO sample appears to be most similar to main-sequence galaxies at $z \sim 1-2$ (Chapman et al. 2003), which we show in Fig. 4. We highlight that Chapman et al. (2003) is the only sample that overlaps with DYNAMO galaxies in both L_{IR} and T_{dust} . This is yet again an example of the similarity between DYNAMO galaxies and $z \sim 1-2$ main-sequence disks.

Dust temperature is frequently used as an indicator of CO conversion factor (reviewed in Bolatto 2015). The dust temperatures we measure, therefore, also provide practical information about measuring gas mass via CO[1-0] flux on similar galaxies in DYNAMO. We find dust temperatures $\sim 27\text{K}$ for our DYNAMO-Herschel sample. Magnelli et al. (2012) suggest a critical value for T_{dust} of $\sim 30\text{K}$ (see also Solomon et al. 1997; Tacconi et al. 2008). For SFGs that are dominated by self-gravitating giant molecular clouds and which generally have colder dust temperatures ($< 30\text{K}$) they prescribe a Milky Way-like value for α_{CO} . For systems

observed with hotter dust ($>30\text{K}$) their results suggest $\alpha_{\text{CO}} = 1 M_{\odot} (\text{K km s}^{-1} \text{pc}^2)^{-1}$ may be more appropriate. We note that those few galaxies that have both IR and CO data measure very consistent gas masses through these independent methods (similar to results of Genzel et al. 2015 for high- z main-sequence galaxies). Moreover, Fisher et al. (2014) finds a similar, Milky Way-like, α_{CO} for DYNAMO galaxies using the stellar mass surface density (as prescribed in Bolatto et al. 2013). It therefore appears that all efforts to constrain CO-to- H_2 conversion factors in DYNAMO disks are consistent with our choice of α_{CO} in §3.1.1 (Equation 2).

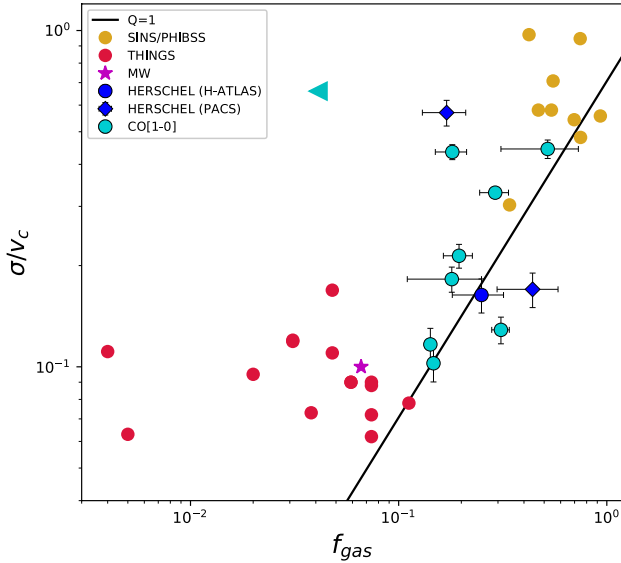


Figure 5. The ratio between mean velocity dispersion to rotational velocity plotted against the molecular gas mass fraction (f_{gas} ; using CO-derived values where possible). We include the 3 detected systems from Fisher et al. (2014). To place these DYNAMO galaxies (blue and cyan, with upper limit value for G13-1 as leftward arrow) in context, we include nearby disk galaxies from the THINGS survey (in red; Walter et al. 2008; Ianjamasimanana et al. 2012) and high- z star forming galaxies observed as part of PHIBSS (in gold, kinematics from SINS; Genzel et al. 2013; Förster Schreiber et al. 2009). The solid line corresponds to the relationship between f_{gas} and σ/v_c derived in the text, assuming instability theory (Eq. 10).

4.2. σ/v_c vs f_{gas}

We utilize the kinematic information from DYNAMO-I to investigate this relationship between the molecular gas content and dispersion within the disks in Fig. 5. The DYNAMO sample in this figure is constructed from the 9 unique galaxies from this paper with kinematics and 3 detected systems from Fisher et al. (2014), utilizing CO-derived f_{gas} values where possible. Nearby disk galaxies from The HI Nearby Galaxy Survey (THINGS, seen in red, where we have excluded dwarf galaxies and selected out systems with $M_{\text{star}} > 10^9 M_{\odot}$; Walter et al. 2008; Ianjamasimanana et al. 2012) and high- z star forming galaxies observed as part of IRAM Plateau de Bure High- z Blue Sequence Survey (PHIBSS; seen in green,

with kinematics from the SINS survey; Tacconi et al. 2013; Genzel et al. 2013; Förster Schreiber et al. 2009) have been included to place the DYNAMO results (blue and cyan for Herschel and PdBI, respectively) in context. Note that we have added in a 10 km/s correction for thermal broadening to the sigma values for THINGS galaxies. The DYNAMO data fills in parameter space between the high f_{gas} and σ/v_c values reported in PHIBSS-SINS ($z > 2$) galaxies and the low- z THINGS galaxies. DYNAMO data therefore is necessary to identify the $f_{\text{gas}}-\sigma/v_c$ relationship as a one-to-one correlation as opposed to two distinct groupings in parameter space.

We find that the data set in Fig. 5 has a Pearson’s correlation coefficient of $r=0.77$ (note: in our fit, we exclude our upper-limit values and the two, low- f_{gas} outliers in THINGS). The best fit relationship to the data in Fig. 5 returns a sub-linear slope, however with very large scatter. We find $\log(\sigma/v_c) \propto 0.7 \pm 0.6 \times \log(f_{\text{gas}}) - 0.07 \pm 0.35$. We acknowledge that for a different choice of α_{CO} , this correlation would not hold.

The correlation we observe in Fig. 5 has been assumed, or predicted, by a number of previous authors when invoking marginal stability models of disks (e.g. Swinbank et al. 2012; Genzel et al. 2013; Glazebrook 2013). In this model the stability of rotationally-supported disks ($v_c/\sigma \geq 1$) is represented by Toomre’s Q parameter (Toomre 1964):

$$Q_{\text{gas}} = \frac{\sqrt{2}v_c\sigma}{\pi Gr\Sigma_{\text{gas}}} \quad (7)$$

where we have assumed a flat rotation curve. In this relation, v_c is the circular velocity, Σ_{gas} is the surface density of the gas at radius r and defined as:

$$\Sigma_{\text{gas}} = \frac{M_{\text{gas}}(r)}{\pi r^2} \quad (8)$$

and we have taken σ to be the local vertical gas velocity dispersion.

Using $v_c^2 = \frac{GM_{\text{tot}}(r)}{r}$ and defining $f_{\text{gas}} = \frac{M_{\text{gas}}(r)}{M_{\text{tot}}(r)}$, then Toomre’s Q_{gas} can be expressed as:

$$Q_{\text{gas}} = \sqrt{2} \frac{\sigma}{v_c} \frac{1}{f_{\text{gas}}} \quad (9)$$

A direct relationship between σ/v_c and f_{gas} (we note that this relation has been previously predicted by Genzel et al. 2011 and Glazebrook 2013) emerges when we set $Q_{\text{gas}}=1$ (the instability condition):

$$\frac{\sigma}{v_c} = \frac{f_{\text{gas}}}{\sqrt{2}} \quad (10)$$

The consistency between gas fraction and kinematics (as given in Eq. 10) has important implications for disk properties and the role that this gas rich mode of star formation plays in defining galaxy structure. As the dynamical timescale within a typical disk is of order $t_{\text{dyn}} \sim 10$ Myr, we can assume that the gas within the disk is in hydrostatic equilibrium (e.g. $\frac{dP}{dz} = -\rho g_z$, where P is the pressure and g_z is the vertical component of gravity). Then, using Gauss’ Law for the gravitational contribution due to the gas one can show that:

$$g_{z,gas} = 2\pi G \Sigma_g \quad (11)$$

where as the stars and dark matter contribute (Binney & Tremaine 2008):

$$g_{z,stars+DM} = \frac{v_c^2}{r} \frac{z}{r} (1 - f_{gas}). \quad (12)$$

If one assumes that the pressure is entirely the result of turbulent motions of the gas (e.g. $P = \rho \sigma^2$), which extend above some scale height $z=H$, then:

$$\frac{dP}{dz} \approx \frac{\rho \sigma^2}{H}. \quad (13)$$

Setting Eq. 10 equal to the condition for hydrostatic equilibrium (where $g_z = g_{z,gas} + g_{z,stars+DM}$) one finds that:

$$\frac{\sigma}{v_c} \approx \frac{H}{r}. \quad (14)$$

This result can be inserted into Eq. 10 ($Q_{gas}=1$) to find:

$$f_{gas} = \frac{\sqrt{2}H}{r}. \quad (15)$$

This presents an important, physical explanation for the results presented in Fig. 5: in a marginally stable disk, higher gas fractions naturally lead to thicker disks. This is consistent with Glazebrook 2013 where they show (via similar arguments) that the disk thickness is of order the Jeans length (this is also predicted in simulations; see Bournaud et al. 2009). Moreover, Bassett et al. (2014) find that stellar velocity dispersions in DYNAMO disks are high, implying that turbulent motions build thick disks.

4.3. Depletion times for DYNAMO galaxies

In the local universe there is a mild variation in global depletion times ($t_{dep} = M_{mol}/\text{SFR}$) on galaxy mass (Saintonge et al. 2011b). At the ~ 1 kpc scale, depletion times are found to be roughly constant in disk galaxies (~ 1 Gyr; Leroy et al. 2008; Bigiel et al. 2008; Rahman et al. 2012). At high redshift this value is more uncertain. For main-sequence systems around $z \sim 1.5 - 2$ the average depletion time is a factor of 3-5 below the local spiral value (Daddi et al. 2010; Tacconi et al. 2013). In this paper we find DYNAMO galaxies have a range of depletion times from $\sim 0.5 - 5$ Gyr. In Table 2, we list the depletion times for our targets.

Galaxies G20-2, G14-1, and G08-5 from our sample all have depletion times below 1 Gyr (see Table 2; D00-1 is consistent with 1 Gyr). These galaxies all have significantly higher σ/v_c ratios (respectively $\sigma/v_c = 0.21, 0.44,$ & 0.33) than both the rest of the DYNAMO sample and the THINGS sample. Guo et al. (2015) argues that the ‘‘clumpiness’’ of a galaxy is best defined by the maximum clump flux normalized by the galaxy flux observed within a target. Using this metric, we find that G20-2, G14-1, G08-5 have $L_{clump,max}/L_{total} = 0.1, 0.3,$ and 0.1 respectively (Fisher et al. 2017b).

Conversely, we observe longer depletion times for galaxies C13-1, D15-3 and D13-5 ($t_{dep} > 1$ Gyr). These

three longer depletion time systems have both lower values of σ/v_c (0.12, 0.10, and 0.18, respectively), and significantly less prominent clumps ($L_{clump,max}/L_{total} = 0.02, 0.03,$ and 0.08).

In Fig. 6, we provide high-resolution HST H α maps for seven DYNAMO galaxies (G08-5, G14-1, G20-2, D13-5, G04-1, D15-3, and C13-1) with inferred depletion times to further illustrate this emerging trend between depletion time and clump prominence.

Our data thus far is consistent with lower gas depletion time galaxies having larger, more pronounced clumps and more turbulent gas (as indicated by higher ratios of σ/v_c). Nonetheless, this result should be taken as merely suggestive. In an forthcoming paper we intend to investigate this possible trend with a larger data set of NOEMA observations and ionized gas maps (Fisher et al *in prep*).

5. SUMMARY

In this paper, we present gas mass estimates for a unique sample of 13 local galaxies ($z \sim 0.07$ & 0.1) whose kinematic and star forming properties closely resemble that observed in $z \approx 1.5$ star forming disks.

- Six DYNAMO galaxies have been observed with the Plateau de Bure interferometer and targeting the CO[1-0] transition line (Fig. 1). Five are well-detected at $> 8\sigma$ yielding CO fluxes and line luminosities consistent with gas mass fractions up to $\sim 30\%$, assuming $\alpha_{CO} = 3.1 M_{\odot} (\text{K km s}^{-1} \text{pc}^2)^{-1}$.
- Fitting a modified blackbody function to existing Herschel IR observations (from PACS+SPIRE, Fig. 2) for 9 additional galaxies, we find that the dust within these galaxies is substantial ($M_{dust}; 1-3 \times 10^9 M_{\odot}$) and cold ($T_{dust} < 30\text{K}$, Fig. 3). Using a locally-derived dust-to-gas ratio (D:G ~ 0.01) our fitted M_{dust} predict high gas masses ($f_{gas} \sim 10-40\%$) for our Herschel sample.
- We confirm the gas-rich nature of DYNAMO galaxies with a sample that is $\sim 5x$ larger than previous work and via multiple methods to reduce observational bias.
- Coupling the gas mass fractions with existing high-resolution kinematics in DYNAMO we report a linear relationship between f_{gas} and σ/v_c (see Fig. 4). Predicted from Toomre instability theory, this provides direct observational evidence of the role performed by the internal velocity dispersion of the gas in the formation of massive star forming clumps within galaxies.
- We find that DYNAMO systems with depletion times most consistent with that of high- z star forming disks ($t_{dep} \sim 0.5$ Gyr) also exhibit the highest ratios of σ/v_c and (when imaging is available) very prominent clumps within their disks.

ACKNOWLEDGEMENTS

The science done above is based on data obtained at the Plateau de Bure millimetre interferometer, which is operated by the Institute for Radio Astronomy in the

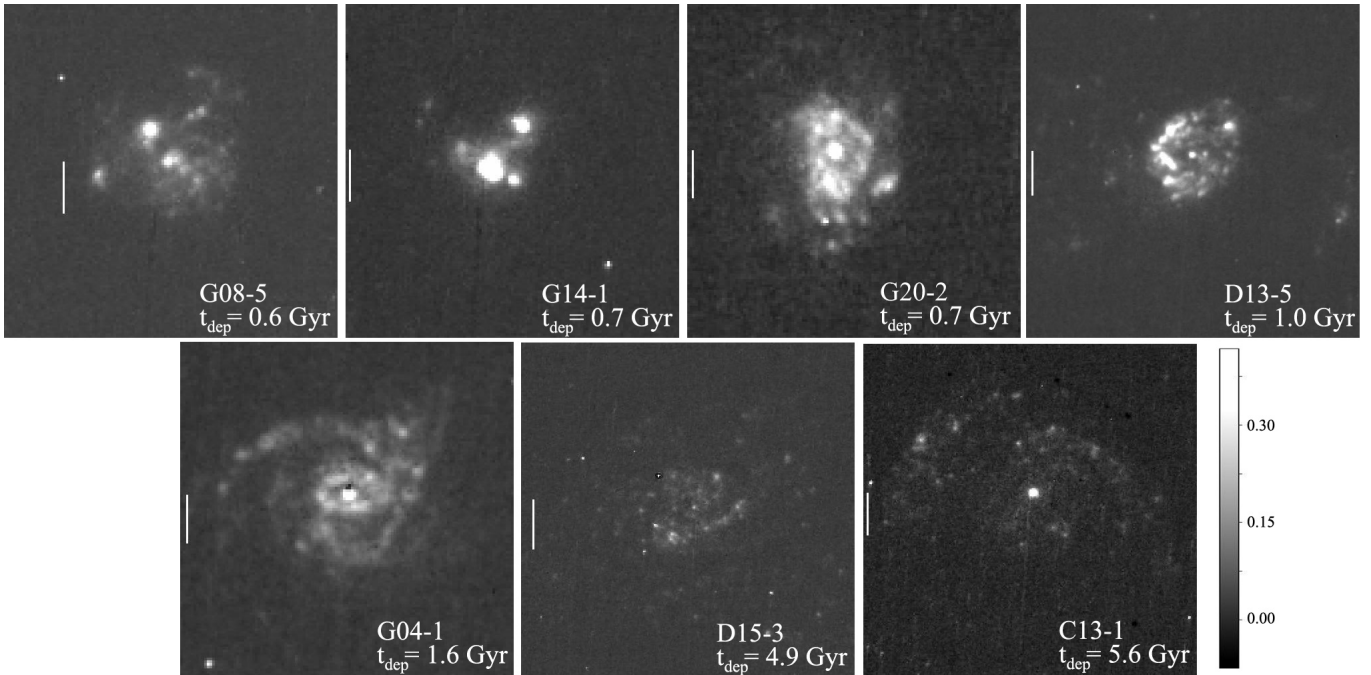


Figure 6. High-resolution $H\alpha$ mapping (obtained using HST’s Wide Field Camera on the Advanced Camera for Surveys (WFC/ACS); reproduced from Fisher et al. 2017b) of seven galaxies in DYNAMO. Galaxy maps are presented in order of increasing inferred depletion time. In this figure, we illustrate a developing trend evidenced in DYNAMO: galaxies with the shortest depletion times exhibit more prominent star forming clumps within their disks. The vertical, white bars in each of the seven panels above, represent ~ 1 kpc on-sky and have been included for scale.

Millimetre Range (IRAM), which is funded by a partnership of INSU/CNRS (France), MPG (Germany), and IGN (Spain) and the Australian Astronomical Observatory and the Australian National University’s 2.3 meter telescope. We also include observations performed with the ESA *Herschel* Space Observatory (Pilbratt et al. 2010), in particular employing *Herschel*’s large telescope and powerful science payload to do photometry using the PACS (Poglitsch et al. 2010) and SPIRE (Griffin et al. 2010) instruments.

HAW and RGA thank NSERC and the Dunlap Institute for Astronomy and Astrophysics for financial support. The Dunlap Institute is funded through an endowment established by the David Dunlap family and the University of Toronto.

DBF and KG acknowledge support from Australian Research Council (ARC) Discovery Program (DP) grant DP130101460. Support for this project is provided in part by the Victorian Department of State Development, Business and Innovation through the Victorian International Research Scholarship (VIRS).

REFERENCES

- Auld, R., et al. 2013, *MNRAS*, 428, 1880
 Balog, Z., et al. 2014, *Experimental Astronomy*, 37, 129
 Bassett, R., et al. 2014, *MNRAS*, 442, 3206
 Bekiaris, G., Glazebrook, K., Fluke, C. J., & Abraham, R. 2016, *MNRAS*, 455, 754
 Berta, S., Lutz, D., Genzel, R., Förster-Schreiber, N. M., & Tacconi, L. J. 2016, *A&A*, 587, A73
 Bianchi, S. 2013, *A&A*, 552, A89
 Bigiel, F., Leroy, A., Walter, F., Brinks, E., de Blok, W. J. G., Madore, B., & Thornley, M. D. 2008, *AJ*, 136, 2846
 Binney, J., & Tremaine, S. 2008, *Galactic Dynamics: Second Edition* (Princeton University Press)
 Bolatto, A. D. 2015, ArXiv e-prints
 Bolatto, A. D., Wolfire, M., & Leroy, A. K. 2013, *ARA&A*, 51, 207
 Boselli, A., et al. 2012, *A&A*, 540, A54
 Bournaud, F., & Elmegreen, B. G. 2009, *ApJ*, 694, L158
 Bournaud, F., Elmegreen, B. G., & Martig, M. 2009, *ApJ*, 707, L1
 Bourne, N., et al. 2016, *MNRAS*, 462, 1714
 Catinella, B., & Cortese, L. 2015, *MNRAS*, 446, 3526
 Chapman, S. C., Helou, G., Lewis, G. F., & Dale, D. A. 2003, *ApJ*, 588, 186
 Cortese, L., et al. 2012, *A&A*, 540, A52
 Daddi, E., et al. 2010, *ApJ*, 713, 686
 Dekel, A., Sari, R., & Ceverino, D. 2009, *ApJ*, 703, 785
 Draine, B. T., & Li, A. 2007, *ApJ*, 657, 810
 Dunne, L., Eales, S., Edmunds, M., Ivison, R., Alexander, P., & Clements, D. L. 2000, *MNRAS*, 315, 115
 Eales, S., et al. 2010, *PASP*, 122, 499
 Elmegreen, D. M., Elmegreen, B. G., Marcus, M. T., Shahinyan, K., Yau, A., & Petersen, M. 2009, *ApJ*, 701, 306
 Fisher, D. B., et al. 2014, *ApJ*, 790, L30
 —. 2017a, *ApJ*, 839, L5
 —. 2017b, *MNRAS*, 464, 491
 Förster Schreiber, N. M., et al. 2009, *ApJ*, 706, 1364
 Galametz, M., et al. 2013, *MNRAS*, 431, 1956
 Garland, C. A., Pisano, D. J., Mac Low, M.-M., Kreckel, K., Rabidoux, K., & Guzmán, R. 2015, *ApJ*, 807, 134
 Genzel, R., et al. 2008, *ApJ*, 687, 59
 —. 2011, *ApJ*, 733, 101
 —. 2013, *ApJ*, 773, 68
 —. 2015, *ApJ*, 800, 20
 Glazebrook, K. 2013, *PASA*, 30, e056
 Green, A. W., et al. 2010, *Nature*, 467, 684
 —. 2014, *MNRAS*, 437, 1070
 Griffin, M. J., et al. 2010, *A&A*, 518, L3
 Guilloteau, S., & Lucas, R. 2000, in *Astronomical Society of the Pacific Conference Series*, Vol. 217, *Imaging at Radio through Submillimeter Wavelengths*, ed. J. G. Mangum & S. J. E. Radford, 299
 Guo, Y., et al. 2015, *ApJ*, 800, 39
 Hopkins, A. M., & Beacom, J. F. 2006, *ApJ*, 651, 142
 Hwang, H. S., et al. 2010, *MNRAS*, 409, 75
 Ianjamasimanana, R., de Blok, W. J. G., Walter, F., & Heald, G. H. 2012, *AJ*, 144, 96
 Kennicutt, R. C., & Evans, N. J. 2012, *ARA&A*, 50, 531
 Kovács, A., Chapman, S. C., Dowell, C. D., Blain, A. W., Ivison, R. J., Smail, I., & Phillips, T. G. 2006, *ApJ*, 650, 592
 Lee, J. C., Hwang, H. S., & Ko, J. 2013, *ApJ*, 774, 62

- Lehnert, M. D., Nesvadba, N. P. H., Le Tiran, L., Di Matteo, P., van Driel, W., Douglas, L. S., Chemin, L., & Bournaud, F. 2009, *ApJ*, 699, 1660
- Leroy, A. K., Walter, F., Brinks, E., Bigiel, F., de Blok, W. J. G., Madore, B., & Thornley, M. D. 2008, *AJ*, 136, 2782
- Madau, P., & Dickinson, M. 2014, *ARA&A*, 52, 415
- Magdis, G. E., et al. 2014, *ApJ*, 796, 63
- Magnelli, B., et al. 2012, *A&A*, 548, A22
- Obreschkow, D., & Rawlings, S. 2009, *ApJ*, 696, L129
- Ott, S. 2010, in *Astronomical Society of the Pacific Conference Series*, Vol. 434, *Astronomical Data Analysis Software and Systems XIX*, ed. Y. Mizumoto, K.-I. Morita, & M. Ohishi, 139
- Pilbratt, G. L., et al. 2010, *A&A*, 518, L1
- Poglitsch, A., et al. 2010, *A&A*, 518, L2
- Rahman, N., et al. 2012, *ApJ*, 745, 183
- Rémy-Ruyer, A., et al. 2014, *A&A*, 563, A31
- Saintonge, A., et al. 2011a, *MNRAS*, 415, 32
- . 2011b, *MNRAS*, 415, 61
- Skibba, R. A., et al. 2011, *ApJ*, 738, 89
- Solomon, P. M., Downes, D., Radford, S. J. E., & Barrett, J. W. 1997, *ApJ*, 478, 144
- Swinbank, A. M., Smail, I., Sobral, D., Theuns, T., Best, P. N., & Geach, J. E. 2012, *ApJ*, 760, 130
- Tacconi, L. J., et al. 2008, *ApJ*, 680, 246
- . 2010, *Nature*, 463, 781
- . 2013, *ApJ*, 768, 74
- Toomre, A. 1964, *ApJ*, 139, 1217
- Walter, F., Brinks, E., de Blok, W. J. G., Bigiel, F., Kennicutt, Jr., R. C., Thornley, M. D., & Leroy, A. 2008, *AJ*, 136, 2563
- Wisnioski, E., et al. 2011, *MNRAS*, 417, 2601
- . 2015, *ApJ*, 799, 209
- Wright, E. L., et al. 2010, *AJ*, 140, 1868
- Yang, M., Greve, T. R., Dowell, C. D., & Borys, C. 2007, *ApJ*, 660, 1198

Table 1
IR and Radio Observations of DYNAMO Galaxies

<i>Herschel</i> PACS+SPIRE Galaxy	$70\mu m$	$100\mu m$	$160\mu m$	$250\mu m$	$350\mu m$	$500\mu m$	T_{dust} (K)	M_{dust}
C08-2	-	0.393 ± 0.043	0.356 ± 0.045	0.188 ± 0.006	0.082 ± 0.007	0.023 ± 0.008	26.63 ± 0.93	3.82 ± 0.37
I09-1	-	0.707 ± 0.041	0.75 ± 0.048	0.398 ± 0.006	0.176 ± 0.007	0.057 ± 0.008	25.39 ± 0.43	105.12 ± 5.05
C14-2	-	0.18 ± 0.041	0.26 ± 0.048	0.095 ± 0.007	0.038 ± 0.008	0.015 ± 0.008	26.6 ± 1.79	1.83 ± 0.36
D14-1	-	0.484 ± 0.041	0.466 ± 0.048	0.198 ± 0.007	0.081 ± 0.008	0.044 ± 0.009	28.09 ± 0.86	5.89 ± 0.52
G14-1	-	0.119 ± 0.041	0.112 ± 0.048	0.047 ± 0.007	0.021 ± 0.008	-0.005 ± 0.009	29.07 ± 3.74	4.39 ± 1.65
D00-2	0.195 ± 0.001	-	0.299 ± 0.027	-	-	-	28.18 ± 0.64	5.08 ± 0.84
D13-5	0.598 ± 0.061	-	0.803 ± 0.154	-	-	-	29.13 ± 1.66	10.44 ± 3.81
D15-3	0.187 ± 0.016	-	0.424 ± 0.009	-	-	-	25.64 ± 0.52	6.68 ± 0.55
G03-2	0.072 ± 0.012	-	0.111 ± 0.011	-	-	-	28.11 ± 1.36	5.16 ± 1.18

PdBI CO[1-0]	t_{int} (hr)	A_{beam}	Δv (km s $^{-1}$)	F_{CO}^c	L_{CO}^d	M_{gas}^a
C13-1	1.05	$5.94''\times 4.19''$	196.4	5.84 ± 0.15	1.91 ± 0.05	0.59 ± 0.02
G20-2	0.90	$9.46''\times 4.71''$	237.4	1.57 ± 0.18	1.68 ± 0.19	0.52 ± 0.06
G13-1	1.99	$5.94''\times 4.64''$	-	0.149^\dagger	0.155^\dagger	0.048^\dagger
G14-1	1.09	$7.13''\times 4.66''$	235.6	1.69 ± 0.20	1.594 ± 0.19	0.49 ± 0.06
G08-5	1.05	$5.36''\times 4.47''$	353.3	2.44 ± 0.27	2.29 ± 0.26	0.71 ± 0.08
D15-3	1.46	$6.26''\times 4.44''$	360.8	12.8 ± 0.25	3.02 ± 0.06	0.94 ± 0.02

^a Dust masses are in units of 10^7 . All other masses are stated in units of $10^{10} M_\odot$.

^b All Herschel waveband fluxes in Jy.

^c Integrated flux density (F_{CO}) in units of Jy km s $^{-1}$.

^d CO line luminosity in units of 10^9 K km s $^{-1}$ pc 2 .

[†] Denotes quantities derived from 2σ upper limit flux values.

Table 2
Properties of DYNAMO Galaxies

Galaxy	M_* ($10^{10}M_\odot$)	z	SFR _{WISE} ($M_\odot\text{yr}^{-1}$)	σ/v_c	Method	M_{gas} (10^9M_\odot)	f_{gas}	M_{dyn} (10^9M_\odot)	t_{dep} (Gyr)
C08-2	1.09	0.0581	1.86	-	Dust	3.82 ± 0.37	0.26	-	2.05 ± 0.72
I09-1	25.2	0.1818	15.6	-	Dust	105 ± 5.1	0.29	-	6.72 ± 1.99
C14-2	0.56	0.0562	1.12	0.16 ± 0.02	Dust	1.83 ± 0.36	0.25	34.91	1.63 ± 0.52
D14-1	2.04	0.0736	4.12	-	Dust	5.89 ± 0.52	0.22	-	1.43 ± 0.66
G14-1	2.23	0.1324	6.90	0.44 ± 0.02	Dust	4.39 ± 1.65	0.16	27.63	0.64 ± 0.32
D00-2	2.43	0.0813	5.14	0.57 ± 0.05	Dust	5.08 ± 0.84	0.17	5.33	0.99 ± 0.37
D13-5	5.38	0.0753	6.27	0.18 ± 0.02	Dust	10.4 ± 3.80	0.16	82.95	1.66 ± 1.02
D15-3	5.42	0.0671	1.91	0.10 ± 0.01	Dust	6.69 ± 0.55	0.11	143.1	3.50 ± 1.75
G03-2	0.65	0.1295	4.60	0.17 ± 0.02	Dust	5.16 ± 1.18	0.44	51.15	1.12 ± 0.30
C13-1	3.58	0.0788	1.06	0.12 ± 0.01	CO[1-0]	5.91 ± 0.15	0.14	134.7	5.58 ± 1.81
G20-2	2.16	0.1411	7.79	0.21 ± 0.02	CO[1-0]	5.22 ± 0.59	0.20	30.61	0.67 ± 0.25
G13-1	1.11	0.1388	12.2	0.66 ± 0.03	CO[1-0]	0.48^\dagger	0.04^\dagger	17.36	-
G14-1	2.23	0.1323	6.90	0.44 ± 0.02	CO[1-0]	4.94 ± 0.59	0.18	27.63	0.72 ± 0.25
G08-5	1.73	0.1322	12.2	0.33	CO[1-0]	7.11 ± 0.79	0.30	49.53	0.57 ± 0.21
D15-3	5.42	0.0671	1.91	0.10 ± 0.01	CO[1-0]	9.36 ± 0.18	0.15	143.1	4.89 ± 2.42
D13-5*	5.38	0.0753	6.27	0.18 ± 0.02	CO[1-0]	11.86 ± 0.36	0.18	82.95	1.89 ± 0.94
G04-1*	6.47	0.1298	15.0	0.13 ± 0.01	CO[1-0]	28.99 ± 2.1	0.31	110.5	1.94 ± 0.72
G10-1*	1.22	0.1437	15.7	0.44 ± 0.03	CO[1-0]	13.45 ± 2.15	0.52	17.50	0.86 ± 0.15

[†] Denotes quantities derived from 2σ upper limit flux values.

* Values taken from Fisher et al. (2014). Note: G10-1 does not have an entry in the WISE catalog. For this reason, we use the H α -derived SFR quoted in Green et al. (2014).